第 480 回電波研連 F 分科会
開催日：2003 年 12 月 12 日

Ground-based Polarimetric SAR Data Processing and Monitoring of Seasonal Variations of Trees

Zheng-Shu ZHOU † Wolfgang-Martin BOERNER ‡ and Motoyuki SATO †
† Center for Northeast Asian Studies, Tohoku University, Kawauchi, Sendai, 980-8576, Japan
‡ University of Illinois at Chicago, Communications, Sensing & Navigation Laboratory, Chicago, USA 60607-7018
E-mail: †{zszhou, sato}@cneas.tohoku.ac.jp, ‡wolfgang.m.boerner@uic.edu

Ⅰ. INTRODUCTION

Synthetic aperture radar is usually used for airborne or space borne remote sensing [1]. SAR can also advantageously be exploited in a ground-based radar imaging system. We call it *Ground-based SAR*. It is a new application of the conventional SAR expansion in the spatial domain. A few design options of Ground-based SAR systems were proposed as monitoring tools for agriculture, terrain mapping, a variety of large man-made structures, as well as environmental studies and ground surface deformation detection, including deformation maps of static displacements of a variety of structures like concrete girders in a controlled environment, building models, dams, and bridges, and so on [2-4]. Most of these applications of ground-based SAR were based on interferometric techniques and were developed only for narrow bandwidths. An important feature of electromagnetic radiation is its state of polarization, and a wide range of classification algorithms and inversion techniques have recently been developed based on the transformation of polarization state by scattering objects [1, 5]. Hence, we have extended those earlier approaches and developed an ultra-wideband, ground-based, fully polarimetric SAR system for environmental studies.

This system makes use of a vector network analyzer, one dual-polarized broadband antenna, and a positioner. Testing results show satisfactory polarimetric performance of developed system. Polarimetric calibration obviously improved the features of the GB-SAR system. Using the developed SAR system, we carried out measurements on three different kinds of trees in spring, summer and autumn, respectively. Then, measurements for a cherry tree in three different conditions, namely in buds before blooming, blooming and voluptuous leaves, were contiguously produced. Three-dimensional images were reconstructed from the acquired data by a series of signal processing procedure. By implementing methods of radar polarimetry [2], the ground-based broadband SAR system can be used for monitoring changes in tree structure characteristics, such as the growth of leaves and branches due to seasonal variations. In this report, we describe a ground-based broadband polarimetric SAR system with some experimental performance examinations, present broadband polarimetric GB-SAR data processing algorithms and data interpretations of tree monitoring.

Ⅱ. PERFORMANCE EVALUATION OF GROUND-BASED POLARIMETRIC SAR SYSTEM

Based on SAR principles and simulation results, we developed a broadband, ground-based, fully polarimetric SAR imaging system. The ground-based polarimetric broadband SAR technique is employed for environmental studies by detecting changes in various kinds of vegetation cover due to seasonal variations by our research group [6, 7]. The radar system consisted of a vector network analyzer, a diagonal dual polarized broadband horn antenna, an antenna positioner unit, and a PC-based control unit. The network analyzer, operated in a stepped frequency continuous-wave mode, was used to generate the transmitting signal and to detect scattered signals both in amplitude and phase. The synthetic aperture is realized by scanning the antennas on a horizontal rail and moving along a vertical post. The horizontal and vertical scanning aperture widths determine the horizontal and vertical resolutions. The range resolution depends on the radar frequency and bandwidth [7].

Firstly, we used a metallic sphere as a calibrator to test the radar system. The measurement was carried out in outdoor condition and some absorbing materials were used for reducing reflection from target stand. The theoretical *normalized radar cross section (NRCS*) value shown as the solid line in Fig. 1. The measured data of HH, VV and VH components, compensated by the gain factor of the antenna used in the system, are also plotted in same figure synchronously. We can observe that there are the same number of peaks and that the resonance points of the measured curves coincide with those of the theoretical value shown in Fig. 1. Hence, the measured backscattering data of co-polarization components are consistent and very similar to the theoretical value. The cross-polarization component is about 12 dB lower than co-polarization components.

A modified polarimetric RCS calibration technique using two orientations of the dihedral corner reflectors as calibration targets is introduced [7, 8]. This method is valid for any monostatic or quasi-monostatic radar system. From the theoretical value of two calibrators and measured data, we can recover calibration coefficients. Using the calibration coefficients, the calibrated scattering matrix can be calculated. Table 1 gives the measured scattering

matrices of three standard reflectors and their calibrated scattering matrices. We can find the improvements after calibration, especially in the phase term.

Table 1 Comparison of calibrated scattering matrices with measured scattering matrices

	Measured scattering matrix	Calibrated scattering matrix
Vertical dihedral	$S_{m1}=\begin{bmatrix}0.9813e^{-j113.7^\circ} & 0.0365e^{j129.4^\circ}\\ 0.0365e^{j129.4^\circ} & 1\end{bmatrix}$	$S^c_{m1}=\begin{bmatrix}1.0146e^{-j179.11^\circ} & 0.0657e^{-j101.54^\circ}\\ 0.0657e^{-j102.39^\circ} & 1\end{bmatrix}$
45° dihedral	$S_{m2}=\begin{bmatrix}0.2977e^{j120.4^\circ} & 1\\ 1 & 0.2891e^{j112.3^\circ}\end{bmatrix}$	$S^c_{m2}=\begin{bmatrix}0.1381e^{-j103.82^\circ} & 1\\ 0.9904e^{-j1.43^\circ} & 0.1285e^{-j43.20^\circ}\end{bmatrix}$
Sphere	$S_{m3}=\begin{bmatrix}1 & 0.2331e^{j112.83^\circ}\\ 0.0677e^{j91.76^\circ} & 0.8252e^{-j106.83^\circ}\end{bmatrix}$	$S^c_{m3}=\begin{bmatrix}1 & 0.2454e^{-j23.11^\circ}\\ 0.0806e^{j32.18^\circ} & 0.9345e^{-j21.96^\circ}\end{bmatrix}$

Ⅲ. THREE DIMENSIONAL IMAGING FOR TREE MONITORING

Due to the fact that trees are some of the most important vegetation scatterers in environmental studies, continued data acquisitions were carried out for three different types of trees in three seasons, and for a cherry tree during different situations at two experimental sites. The experimental sites are both located at the Kawauchi Campus, Tohoku University. The experimental site with three different trees is called *Exp#A*. The main targets are denoted by T1, T2 and T3, and represented three different kinds of trees. We have carried out three measurements at the same exact position for the three different trees in late spring (April 19, 2002), in early summer (May 28, 2002) and in late autumn (November 11, 2002), respectively. Table 2 shows the measurement conditions and situations of targets. We used the frequency range from 1 GHz to 5 GHz. It almost covers the L-band to C-band.

Table 2 Condition and target situations for measurements of different tree types

Measurement number	*Exp#A-1*	*Exp#A-2*	*Exp#A-3*
Season	Spring	Summer	Autumn
Weather	Fine	Fine & light windy	Sunny / cloudy & windy
Tree 1 Japanese Zelkova	Bare twigs with bud	Flourishing large leaves	Leaves almost fall off
Tree 2 Japanese cedar	Evergreen	Evergreen	Evergreen
Tree 3 Azalea&Honeysuckle	Bush with fresh leaves	With dense plants	With a few leaves

The target on the second site, *Exp#B,* is a Yoshino cherry tree, one well-known kind of tree in Japan. We have carried out three measurements for a cherry tree too. The three measurements were produced on April 02, 2003 just before the flowers bloomed, on April 14, 2003 with very blooming flowers but no leaves, and on May 27, 2003 with all flowers gone and substantial growth of leaves, respectively. Experimental conditions and target situation for the cherry tree is shown in Table 3. Three polarimetric scattering matrix element data sets, those of HH, VH and VV, were acquired simultaneously.

Table 3 Condition and target situations for measurements of a cherry tree

Measurement number	*Exp#B-1*	*Exp#B-2*	*Exp#B-3*
Season	Spring	Late spring	Early summer
Weather	Fine	Fine	Fine & slightly windy
Yoshino cherry tree	Bare stems with buds	Blooming flowers	Exuberant leaves

3-D Data Processing Algorithms

For the acquired broadband ground-based polarimetric SAR data, a series of signal processing methods are applied. Due to different data structure, ground-based SAR signal processing is not the same as for airborne SAR data processing. First, the acquired frequency domain data are filtered by the broadband-pass filter; then transformed to the time domain by *IFFT*. By selecting the interesting range at time axis, time gating is employed to the time domain data; then back-transformed to the frequency domain by *FFT*. The frequency domain data are calibrated by radar system calibration coefficients. Thereafter, the calibrated data are compressed by matched filtering, in which the

reference signal was the reflection from an aluminum plate measured by the same radar system and parameters. After using the *IFFT* again, the time domain data are obtained. Finally, diffraction stacking is applied to migrate the time domain data while antenna radiation directivity compensation is done synchronously; and the special domain data sets are obtained.

A migration method of diffraction stacking has been employed to reconstruct the image [7]. It is a very convenient and traditional method, which is commonly used for seismic data processing. The goal of migration is to make the stacked section appear similar to the real location. This approach is an integral solution of the wave equation. It can extrapolate wave fields of an observation aperture to larger 3-D space. Diffraction stacking migration produces one migrated sample (a pixel) at a time by computing a diffraction shape for a scatter point at that location, summing and weighting the input energy along a diffraction path, and placing the summed energy at the scatter point location on the migrated section. It makes the data synthesis consistent with the real conditions of the radar system measurement.

The *short time Fourier transform* (*STFT*), also referred to as the *Windowed Fourier Transform*, was developed as an attempt to overcome the lack of information on time locality in Fourier analysis [9]. It is a compromise between the time and the frequency view of a signal, and is thereby better suited for analysis of non-stationary signals than the ordinary Fourier Transform is. STFT computes a time-frequency distribution of an input signal within a given frequency interval as a sequence of short-time spectra of windowed signal segments with constant length.

Reconstructed 3-D Images

Based on measured data of HH, VH and VV polarization, at experimental site *Exp#A*, we have obtained spatial domain data by above processing. Fig. 2 shows the 3-D reconstructed images of HH, VH and VV polarization by three experiments, respectively. Analyzing the three polarimtric images of each measurement, we can find the entire differences among the different polarizations. The HH image shows the reflection from trunks, some horizontal branches and ground clutter, the VH image indicates strong reflections from the leaves and some slant branches and the VV image illustrates the reflections from vertical trunks and branches. Hence, the polarimetretric performance was demonstrated effectively.

Comparing the corresponding images of the different measurement in Fig. 2, we can find the reflections from the trunks and the leaves are different by the seasonal variation. There are stronger reflections in the images of Figs. 2(b1), 2(b2) and 2(b3) due to the exuberant branches and leaves in summer. Moreover, we can find the clearer ground surface in Figs. 2(c1), 2(c2) and 2(c3) in autumn, which agreed well with the real situation. The differences have existed between Figs. 2(a1) and 2(c1), 2(a3) and 2(c3), too. Hence, we can assume that the main reflections were caused by the volume scattering due to the different volumes of leaves in variant season. Although the shapes of trees were very similar in spring and autumn, but the water content of trees was higher than that in autumn. That caused the slight differences between the reconstructed polarimetric images in spring and autumn. The different scattering performances of the variant trees in the different seasons can be observed generally.

Ⅳ. DATA INTERPRETATION WITH SAR POLARIMETRIC ANALYSIS

Polarimetric Power Density Images from Covariance Matrix

For deterministic scatterers, deterministic scattering or completely polarized scattering can be completely described by the coherent Sinclair matrix. But for partial scatterers, random scattering or partially polarized scattering, they can not be described by the Sinclair matrix. The statistical descriptions are necessary such as using the Kennaugh or the Covariance matrices. Hence, the Coherency matrix and the Covariance Matrix maybe usefully employed as target polarimetric descriptors [10].

This coherent Sinclair scattering matrix S is a function of frequency and relative viewing angle.

$$S = \begin{bmatrix} S_{HH} & S_{HV} \\ S_{VH} & S_{VV} \end{bmatrix} \tag{1}$$

The covariance matrix is based on the components of the scattering matrix (1). We have limited our focus to the backscatter (or monostatic) case only. Therefore, the Covariance matrix is defined as:

$$C_{VH} = \left\langle hh^{*T} \right\rangle = \begin{bmatrix} <|S_{HH}|^2> & <\sqrt{2}S_{HH}S_{VH}^*> & <S_{HH}S_{VV}^*> \\ <\sqrt{2}S_{VH}S_{HH}^*> & <2|S_{VH}|^2> & <\sqrt{2}S_{VH}S_{VV}^*> \\ <S_{VV}S_{HH}^*> & <\sqrt{2}S_{VV}S_{VH}^*> & <|S_{VV}|^2> \end{bmatrix} \tag{2}$$

The superscript * denotes the complex conjugate. The superscript *T* means transpose.

Complex spatial frequency domain data are produced from migrated spatial domain data by FFT. Hence, the polarimetric power density images based on diagonal terms of the covariance matrix of (2) for *Exp#B-2* data (cherry flowers) and *Exp#B-3* (cherry leaves) are shown in Fig. 3. The scene of cherry flowers and leaves are shown in Fig.

3(a) and 3(f). Power density images of cherry flowers with frequencies of 1.5 GHz, 2.5 GHz, 3.5 GHz and 4.5 GHz are shown on the left side of Fig. 3. The scene and images of cherry leaves are shown on the right side of Fig. 3. In lower frequencies images (1.5 GHz and 2.5 GHz), the red color and blue color (co-polarization components) are dominant. The reason is that the lower frequency electromagnetic wave can propagate into the canopy of the cherry tree and reflect back against large horizontal and vertical branches. With frequency increased, the green color appears more and more, and becomes dominant. The fact is the higher frequency electromagnetic wave return from the smaller scatterers like inclined twigs, flowers or leaves. Comparing images of flowers and leaves, we can find that a little more green color appear in cherry tree leaves images of higher frequencies (3.5 GHz and 4.5 GHz). The reason may be assumed that the volume of the cherry tree leaves is greater than that of cherry flowers and there are larger scattering surface areas with randomly oriented leaves.

Ⅴ. CONCLUSIONS

In this report, the development of a broadband ground-based polarimetric SAR system and its application to tree monitoring are presented. Testing results and polarimetric calibration showed satisfactory polarimetric performances and improvement of the developed system.

Algorithms of time gating, matched filtering and diffraction stacking were very effective techniques for ground-based SAR data processing. Reconstructed 3-D images of HH, VH and VV polarization components showed good consistency with ground-truths and polarimetry theory. Hence, radar polarimetry provided valuable scattering information about targets, particularly the scattering features of trees in different seasons, so that the different components of trees in different periods could be distinguished.

Different analysis tools for viewing and interpreting broadband polarimetric SAR data were used. Those could indicate scattering mechanisms for vegetation. Scattering mechanisms of different components of vegetation, e.g. trees, were demonstrated by polarimetric analysis techniques. We also discussed, using different data acquired for different cases to interpret the amount of diffuse scattering, for instance, for buds, flowers and leaves. It showed that they all provide similar information but different features could be identified by polarimetric analysis.

It was demonstrated that the broadband ground-based polarimetric SAR system presents advantages for vegetation monitoring as well as environmental studies for a great variety of vegetation structures. At the same time, a ground-based SAR system also can be used as ground truth demonstration tool for airborne SAR and space-borne SAR in a great variety of applications.

ACKNOWLEDGEMENT

A part of this work was supported by the Grant-In-Aid for Scientific Research (S)14102024.

REFERENCES

[1] W.-M. Boerner et al, “Polarimetry in Remote Sensing: Basic and Applied Concepts,” Chapter 5 in *Manual of Remote Sensing*, 3rd ed., vol. 2, F M Henderson, A J Lewis Ed. New York: Wiley, pp. 271-358, 1998.

[2] D. Tarchi, E. Ohlmer and A. Sieber, “Monitoring of Structural Changes by Radar Interferometry,” *Research in Nondestructive Evaluation*. vol. 9, pp. 213-225, 1997

[3] M. Pieraccini, G. Luzi and C. Atzeni, “Terrain Mapping by Ground-Based Interferometric Radar,” *IEEE Trans. Geosci. Remote Sensing*, vol. 39, no. 10, pp. 2176-2181, Oct. 2001

[4] D. Tarchi, H. Rudole, M. Pieraccini and C. Atzeni, “Remote Monitoring of Buildings Using a Ground-Based SAR: Application to Cultural Heritage Survey,” *Int. J. Remote Sensing,* vol. 21, no. 18, pp. 3545-3551, 2000

[5] E. Pottier, S. R. Cloude and W.-M. Boerner, “Recent Development of Data Processing in Polarimetric and Interferometric SAR; Invited Paper, Radio Science Bulletin,” (ed. R.W. Stone), *Special Issue on URSI-GA-03*; Maastricht; NL, RSB-304, March 2003, pp. 48-59, ISSN 1024-4530.

[6] Z.-S. Zhou, and M. Sato, “Ground-Based Polarimetric SAR Systems for Environment Study”, IEEE AP-S 2003 Digest, vol. 1, pp.202-205, Columbus, June 2003.

[7] Z.-S. Zhou, *Application of a Ground-based Polarimetric SAR System for Environmental Study,* Doctoral Dissertation of Tohoku University, Japan, August 2003.

[8] J.-R. J. Gau and W. D. Burnside, “New polarimetric calibration technique using a single calibration dihedral,” *IEE Proc. Microw. Antennas Propag.*, vol. 142, no. 1, February 1995, pp. 19-25.

[9] G. F. Boudreaux-Bartels, “Mixed Time-frequency Signal Transformations,” Chapter 12 in *The Transforms and Applications Handbook,* 2nd ed., A. D. Poularikas Ed, Boca Raton, Florida: CRC Press LLC, 2000, pp. 12.6–12.8.

[10] S. R. Cloude and E. Pottier, “A Review of Target Decomposition Theorems in Radar Polarimetry,” *IEEE Trans. on Geosc. and Remote Sensing*, vol. 34 no. 2 , pp. 498-518, March 1996.

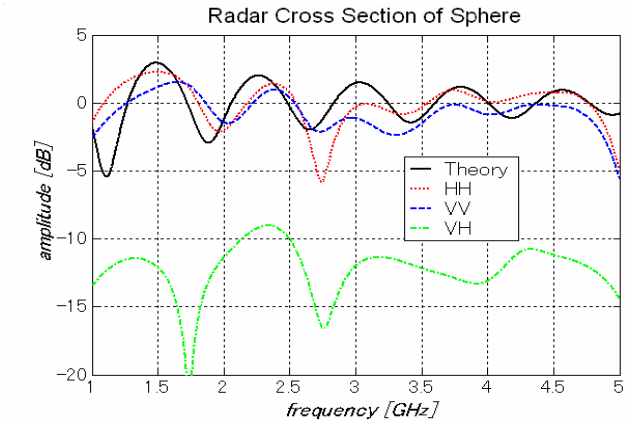

Fig. 1 Theoretical normalized RCS curve and measured values of a metallic sphere: solid line- theoretical curve, dotted line- HH polarization, dashed line- VV polarization and dash-dot line- VH polarization.

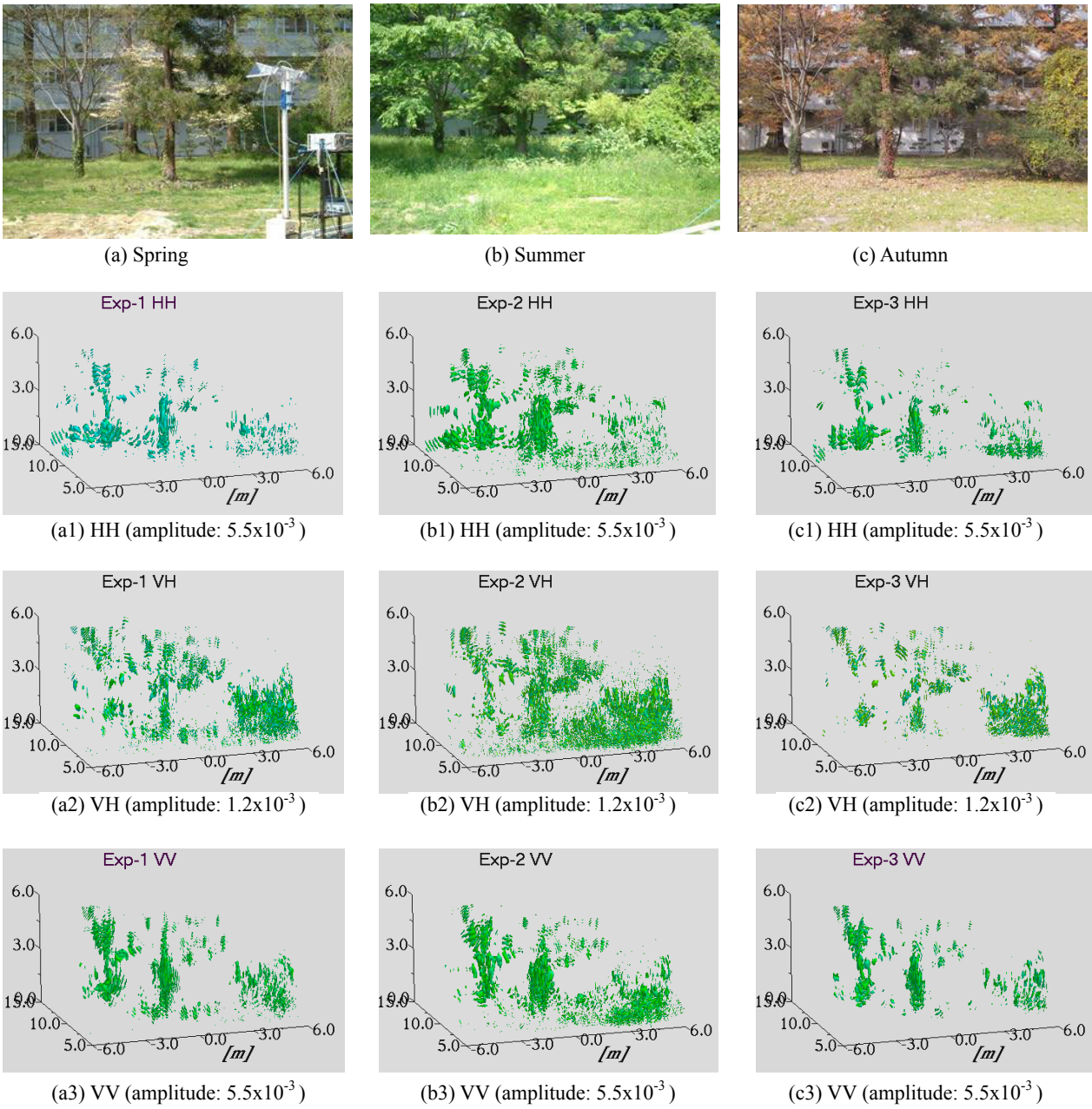

(a) Spring (b) Summer (c) Autumn

(a1) HH (amplitude: 5.5×10^{-3}) (b1) HH (amplitude: 5.5×10^{-3}) (c1) HH (amplitude: 5.5×10^{-3})

(a2) VH (amplitude: 1.2×10^{-3}) (b2) VH (amplitude: 1.2×10^{-3}) (c2) VH (amplitude: 1.2×10^{-3})

(a3) VV (amplitude: 5.5×10^{-3}) (b3) VV (amplitude: 5.5×10^{-3}) (c3) VV (amplitude: 5.5×10^{-3})

Fig. 2 Test scenes and 3-D images of different trees in: (a) spring, (b) summer and (c) autumn.

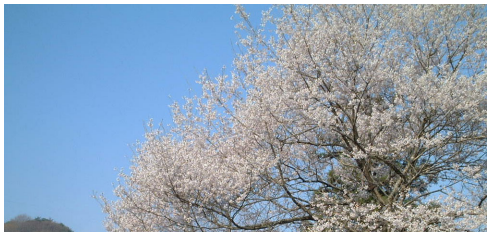

(a) Imaging area of flowers

(f) Imaging area of leaves

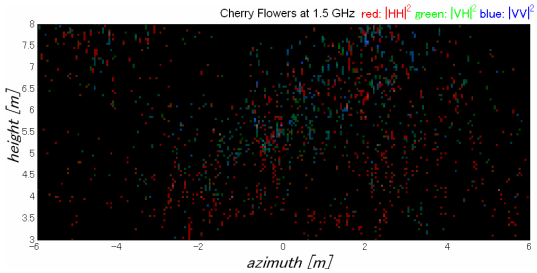

(b) 1.5 GHz

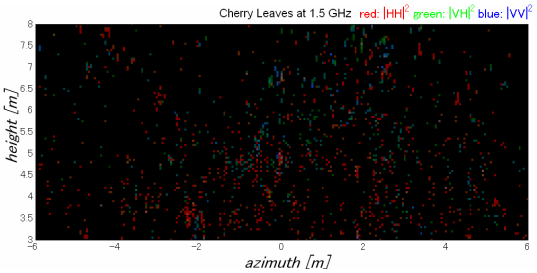

(g) 1.5 GHz

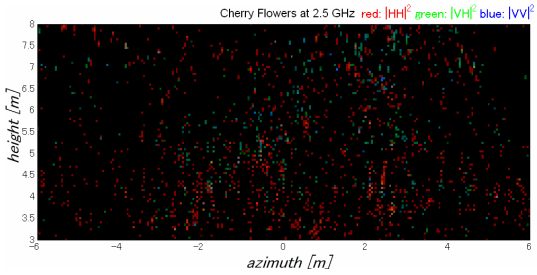

(c) 2.5 GHz

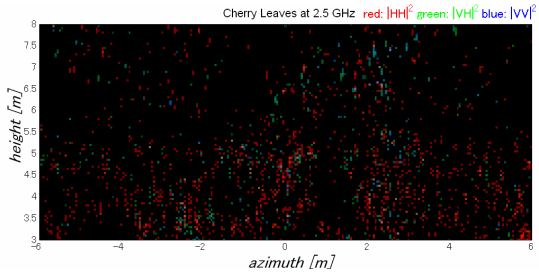

(h) 2.5 GHz

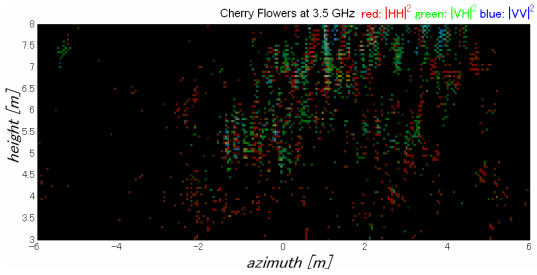

(d) 3.5 GHz

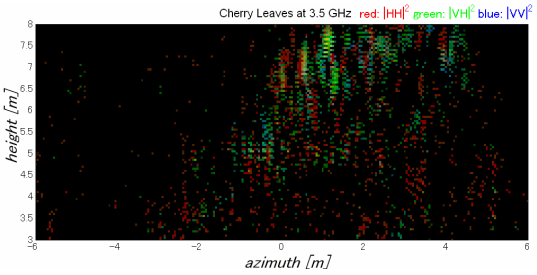

(i) 3.5 GHz

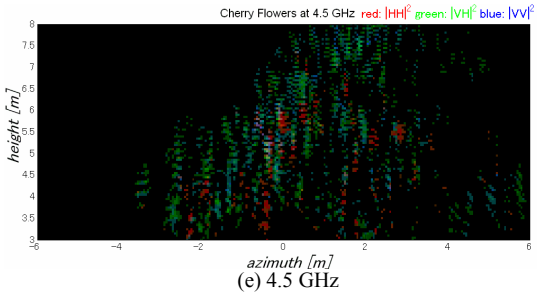

(e) 4.5 GHz

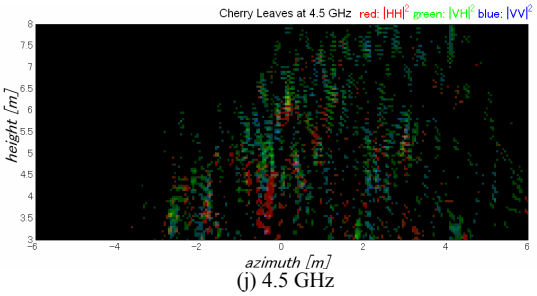

(j) 4.5 GHz

Fig. 3 Single-frequency power density images of cherry blossom and leaves red-$|HH|^2$ green-$2|VH|^2$ blue-$|VV|^2$: (a) imaging area of flowers, (b) 1.5 GHz, (c) 2.5 GHz, (d) 3.5 GHz, (e) 4.5 GHz images of flowers, and (f) imaging area of leaves, (g) 1.5 GHz, (h) 2.5 GHz, (i) 3.5 GHz, (j) 4.5 GHz images of leaves.